

pubs.acs.org/JPCL Letter

# Photoelectron Spectroscopy of Oppositely Charged Molecular Switches in the Aqueous Phase: Theory and Experiment

E. Ikonnikov, M. Paolino, J. C. Garcia-Alvarez, Y. Orozco-Gonzalez, C. Granados, A. Röder, J. Léonard, M. Olivucci, S. Haacke, O. Kornilov,\* and S. Gozem\*



Cite This: J. Phys. Chem. Lett. 2023, 14, 6061-6070



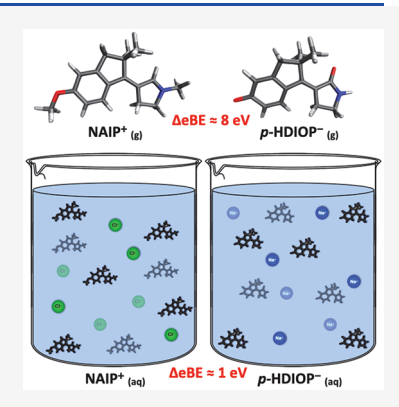
**ACCESS** I

III Metrics & More

Article Recommendations

s) Supporting Information

**ABSTRACT:** XUV photoelectron spectroscopy (XPS) is a powerful method for investigating the electronic structures of molecules. However, the correct interpretation of results in the condensed phase requires theoretical models that account for solvation. Here we present experimental aqueous-phase XPS of two organic biomimetic molecular switches, NAIP and p-HDIOP. These switches are structurally similar, but have opposite charges and thus present a stringent benchmark for solvation models which need to reproduce the observed  $\Delta eBE = 1.1$  eV difference in electron binding energy compared to the 8 eV difference predicted in the gas phase. We present calculations using implicit and explicit solvent models. The latter employs the average solvent electrostatic configuration and free energy gradient (ASEC-FEG) approach. Both nonequilibrium polarizable continuum models and ASEC-FEG calculations give vertical binding energies in good agreement with the experiment for three different computational protocols. Counterions, explicitly accounted for in ASEC-FEG, contribute to the stabilization of molecular states and reduction of  $\Delta eBE$  upon solvation.



WV photoelectron spectroscopy (XPS) is a powerful analytical method to study the electronic structure of molecules. While originally a gas-phase or solid-state surface technique, developments in experimental technologies such as liquid microjets<sup>1,2</sup> and ambient pressure instruments<sup>3</sup> have extended XPS to the solution phase, where many chemical and biological systems reside. The past decade has seen several applications of static XPS to biologically relevant organic molecules<sup>4-6</sup> as well as time-resolved XPS to small inorganic and organic molecules.<sup>7-12</sup>

Experimentally, the interpretation of solution-phase XPS is complicated by several factors. The well-resolved vibronic peaks readily observed in gas-phase spectra are broadened, shifted, and merged together in solution, resulting in broad bands that are more difficult to connect to theoretical quantities, such as vertical binding energies, adiabatic binding energies, and Franck—Condon factors. Scattering and gas—liquid interface effects also complicate the interpretation of the XPS spectra. Predicting solution-phase binding energies from first principles can also be challenging; quantum chemical computations must treat the initial and ionized states of the system in a balanced way and capture both short- and long-range solute—solvent interactions through either a large (or periodic) solvent box, <sup>13–18</sup> nonequilibrium continuum solvation, <sup>19–24</sup> or a mix of explicit and implicit solvation.

Here we report for the first time the experimental XPS spectra and calculated electron binding energies of two molecular switches. The first switch is the methoxy N-alkylindanylidene-pyrrolinium (dMe-MeO-NAIP, from now on referred to as NAIP). This switch is demethylated on C5 of

the pyrroline compared to the previously investigated compound of ref 27. The second switch is para-hydroxydimethylindanylidene-oxopyrrolidine (p-HDIOP). These molecules, shown in Figure 1, are biomimetic switches designed to mimic the ultrafast photoisomerization of the retinal protonated Schiff base (rPSB) chromophore of rhodopsin<sup>27,28</sup> and the anionic chromophore of the green fluorescent protein,<sup>29</sup> respectively. Photoisomerization of these switches occurs on subpicosecond time scales in methanol, within 300 fs for NAIP<sup>30</sup> and 400 fs for p-HDIOP,<sup>29</sup> but with a relatively low quantum efficiency in the 20% range. NMR analysis has shown that before illumination, NAIP is predominantly (>95%) in the E form, 28 and p-HDIOP also adopts the E isomer in the ground state.<sup>29</sup> For the purpose of this study, we consider them as model benchmark systems for studying the effect of solvation on electronic binding energies. Importantly, NAIP and p-HDIOP are structurally similar but are oppositely charged. NAIP is positively charged, becoming a 2+ ion upon photoionization, while p-HDIOP is negatively charged, becoming neutral upon photodetachment. Because of this difference, their electron binding energies are very different in the gas phase. However, the experiments reported in this

Received: March 28, 2023 Accepted: June 20, 2023



Figure 1. Structures of E-NAIP and E-p-HDIOP.

Letter find that this difference is reduced to just 1.1 eV in the aqueous phase due to solvation effects. This poses a challenge to computations, which must capture the large and opposite solvent effect on the binding energies of the two molecules.

# COMPUTATIONAL METHODS

Vertical binding energies ( $E^{\nu}$ ) were first computed using three different electronic structure methods, introduced as M1, M2, and M3 below. The goal of using three methods is not to compare their accuracy but rather to check whether solvation effects computed for those three different methods are generally reproduced.

For each method, we also report adiabatic binding energies  $(E_{ee}^a)$ . Additionally, for method M1 0–0 adiabatic binding energies  $(E_{00}^a)$  are also computed. Figure 2 schematically

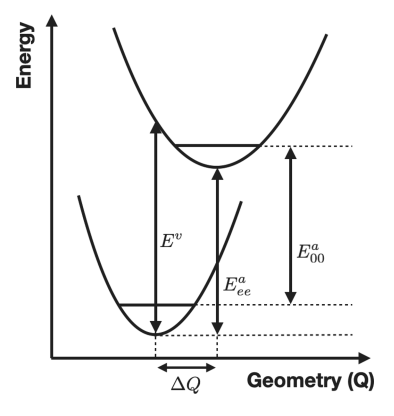


**Figure 2.** Schematic representation of vertical  $(E^v)$ , adiabatic  $(E^a_{ee})$ , and 0–0  $(E^a_{00})$  binding energies.  $\Delta Q$  represents the geometric displacement of the equilibrium structure of the ionized molecule compared with its initial state.

presents the definitions of  $E^{\nu}$ ,  $E^{a}_{ee}$  and  $E^{a}_{00}$ .  $E^{\nu}$  is a difference between the final (ionized) state energy and the initial state energy, both computed at the equilibrium geometry of the initial state.  $E^{a}_{ee}$  is the difference between the final (ionized) state energy and the initial state energy each computed at the equilibrium geometry of the corresponding state.  $E^{a}_{00}$  values are adiabatic energies that account for the zero-point vibrational energy (ZPVE) correction for each state obtained from frequency calculations.

**Method 1 (M1):** Gas-phase geometries and vibrational frequencies were obtained using the PBE0 density functional and 6-311+G\* basis set.  $E^{\nu}$  and  $E^{a}_{ee}$  values were computed using the  $\Delta$ SCF approach.  $E^{a}_{00}$  was computed with  $\Delta$ SCF after taking the sum of the electronic and zero-point vibrational energies for each of the initial and final states at

their respective equilibrium geometries. M1 calculations were carried out with Q-Chem  $5.4.^{33}$ 

Method 2 (M2): Gas-phase geometries were optimized using the ωB97X-D density functional<sup>34</sup> and cc-pVDZ correlation-consistent basis set.<sup>35</sup>  $E^v$  and  $E^a_{ee}$  were computed using equation-of-motion ionization-potential coupled-cluster with single and double excitations (EOM-IP-CCSD) and the cc-pVDZ basis set. EOM-IP-CCSD computes ionized states from a coupled cluster reference wave function at these structures using an electron-annihilating excitation operator.<sup>36,37</sup> To make the calculations tractable, the single-precision implementation<sup>38</sup> of EOM-IP-CCSD and frozen natural orbital (FNO) truncation<sup>39</sup> were employed. M2 calculations were carried out with Q-Chem 5.4.<sup>33</sup>

Method 3 (M3):  $E^{\nu}$  and  $E^{a}_{ee}$  were computed with the secondorder perturbation theory corrected complete-active-space selfconsistent field (CASPT2//CASSCF) method.  $^{40,41}$  Geometry optimizations were carried with CASSCF and the 6-31G\* basis set, while energies of the initial and final (ionized) states were computed using CASPT2 single-point calculations with the ANO-L-VDZP basis set.  $^{56}$  For both molecular switches, an active space of 12 electrons in 11 orbitals was used for the initial state and 11 electrons in 11 orbitals for the ionized state. The CASSCF orbital with single occupancy in the ionized state is shown in Figure 3. In both *E*-NAIP and *E-p*-HDIOP, the

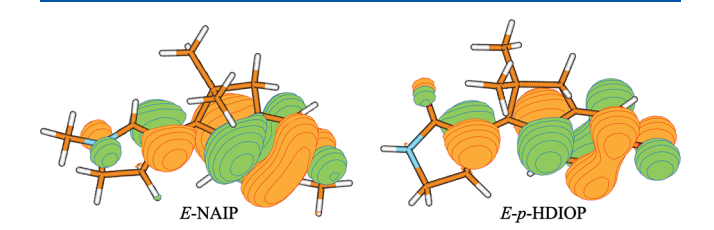


**Figure 3.** CASSCF molecular orbital having a single occupancy for *E*-NAIP (left) and *E-p*-HDIOP (right) in the ionized state. The orbital CASSCF occupancies are between 1.01-1.02. The images were generated using Molden. <sup>59</sup>

ionization occurs from the  $\pi$  orbitals, whether in the gas phase or in solution. No state-averaging was employed for the CASSCF wave function, and a single-state CASPT2 was used for each of the initial and ionized states. The Cholesky decomposition was used for CASPT2. <sup>57</sup> M3 calculations were carried out in OpenMolcas version 22.10. <sup>58</sup>

Methods M1 and M2 or similar protocols have been used in multiple instances for computing electron binding energies, with benchmarks indicating typical errors of 0.1–0.2 eV relative to experiments for molecules that do not have strong electron correlation. 6.17,46–51 The CASPT2//CASSCF ap-

proach has been regularly employed to study NAIP, *p*-HDIOP, and rPSB and has been shown to benefit from a cancellation of errors that makes it suitable for modeling the excitation energies and photoisomerization mechanism of those systems. <sup>29,42–45</sup> CASPT2 and related multireference methods have also been used to compute binding energies accurately in systems ranging from small metal clusters <sup>52,53</sup> to other biologically relevant molecules. <sup>54,55</sup>

Geometry optimizations were carried with CASSCF and the  $6\text{-}31G^*$  basis set, while energies of the initial and final (ionized) states were computed using CASPT2 single-point calculations with the ANO-L-VDZP basis set. For both molecular switches, an active space of 12 electrons in 11 orbitals was used for the initial state and 11 electrons in 11 orbitals for the ionized state. The CASSCF orbital with single occupancy in the ionized state is shown in Figure 3. In both *E*-NAIP and *E-p*-HDIOP, the ionization occurs from the  $\pi$  orbitals, whether in the gas phase or in solution. No state-averaging was employed for the CASSCF wave function, and a single-state CASPT2 was used for each of the initial and ionized states. The Cholesky decomposition was used for CASPT2. M3 calculations were carried out in OpenMolcas version 22.10. Sec.

The effect of solvation on the electron binding energies was computed by using both implicit and explicit solvent models. For M1, the  $E^{\nu}$ ,  $E^{a}_{ee}$  and  $E^{a}_{00}$  calculations were repeated using the conductor-like polarizable continuum model (C-PCM). By default, these models solve for both the fast (e.g., polarization) and slow (e.g., orientational) components of the solvent response. This formulation, labeled equilibrium PCM (e-PCM), was used to compute the adiabatic energies in solvation. e-PCM is not suitable for computing vertical binding energies ( $E^{\nu}$ ), where only the fast component of the solvent polarization remains in equilibrium with the sudden ionization but the slow component is effectively frozen. Therefore, we also computed  $E^{\nu}$  using a nonequilibrium formulation of PCM (ne-PCM) using the Marcus-Brady-Carr state-specific approach.  $E^{\nu}$ 0,20,21,62-64

For M2, EOM-IP-CCSD ne-PCM calculations used a zeroth-order treatment that employs solvent-polarized molecular orbitals for the EOM-IP-CCSD calculations.<sup>64</sup>

Explicit solvent calculations were performed using the average solvent electrostatic configuration and free energy gradient (ASEC-FEG) quantum mechanical/molecular mechanical (QM/MM) approach. The theoretical details of this method have been described previously. 65-73 The details of the model setup and methodology are presented in the Supporting Information. Briefly, the quantum chemical optimization and energy calculations are performed iteratively in the field of a time-averaged environment of the solution obtained from MD snapshots. Water molecules and counterions (Na<sup>+</sup> in the case of p-HDIOP and Cl<sup>-</sup> in the case of NAIP) are included explicitly in the MD and ASEC-FEG QM/MM calculations. Their presence not only ensures a globally neutral system before ionization but also accounts for the electrostatic interaction between the solute and the counterion in an averaged way.  $^{72}$  The ASEC-FEG approach is related to other methods that simulate QM energies in a conformationally sampled solvent environment such as ASEP/MD, 74 MESS-E, 7 and QM-NBB.<sup>76</sup> MD simulations were carried out using GROMACS 2022.3,77,78 while QM/MM calculations were carried out using the OpenMolcas<sup>79</sup> and Tinker 6.3<sup>80</sup> interface,81 treating the molecular switches at the QM level

of theory and the ASEC solvent and counterions at the MM level of theory. The QM subsystem was optimized at the CASSCF/6-31G\* level of theory. As with the gas-phase calculations, CASSCF employed a 12 electron in 11 orbital active space and no state averaging.

For each of p-HDIOP and NAIP, the ASEC configurations (taken from the last iteration of the ASEC-FEG protocol) were exported to Q-Chem, and PBE0/6-311+G\*  $\Delta$ SCF and EOM-IP-CCSD/cc-pVDZ binding energies were computed in that ASEC charge environment.

Test calculations were also carried out where solution ions  $(Na^+ \text{ for } p\text{-HDIOP} \text{ and } Cl^- \text{ for NAIP})$  were deleted for each step of the ASEC-FEG protocol to compute the CASTP2 ionization energies in the absence of ions. The results are labeled as M3-no ion.

Radial distribution functions (RDFs) for the counterions were computed with periodic boundary conditions using the gmx rdf tool in GROMACS. The cumulative number (CN), a normalized integral of the RDF that in this case indicates the probability of finding the counterion within distance r, was also generated.

### **EXPERIMENTAL METHODS**

The two molecular switches were prepared and characterized according to procedures reported in the literature (see ref 82 for NAIP and ref 29 for *p*-HDIOP).

The spectroscopy experiments were performed at the XUV monochromator beamline described previously. <sup>9,11,83</sup> In short, XUV light is produced by high-order harmonic generation (HHG) driven by a Ti:Sa femtosecond multi-mJ laser source with the central wavelength of 795 nm. The HHG spectrum generated in argon is monochromatized by a grating-based grazing incidence monochromator. The monochromator preserves the duration of XUV pulses, which is important for time-resolved experiments performed at the beamline <sup>9,11</sup> but is not relevant for the present static measurements. As described in ref 9, the XUV monochromator beamline is coupled to a microliquid jet endstation equipped with a "magnetic bottle" time-of-flight spectrometer. For the present measurements, harmonic 15 (photon energy of 23.4 eV) was chosen.

As discussed in the literature, 84 determining binding energies in liquid jet photoelectron spectroscopy requires suppression of the streaming potential, which is generated if the solvent has low conductivity. Following earlier work, we added 10 mM NaCl (Sigma-Aldrich) to ultrapure water before preparing sample solutions. The remaining systematic error in the measured photoelectron kinetic energies (e.g., due to incomplete suppression) was eliminated by a calibration procedure using the base solvent solution and harmonics 15 (23.4 eV), 17 (26.4 eV), and 19 (29.6 eV), which allows determining the residual shift of the liquid water 1b, band with respect to the literature value. The photoelectron energy resolution in the experiment is limited by the bandwidth of the source (about 300 meV FWHM83), while the resolution of the time-of-flight spectrometer is better than 100 meV.9 The observed bands in the liquid phase are broadened due to different solvation structures and vibrational excitation upon

It is worth emphasizing that direct comparison of the computed and experimentally determined binding energies is complicated by elastic and inelastic scattering of the photoelectrons by the solvent. Scattering arises from a complex interplay of multiple factors, including solubility of the switches

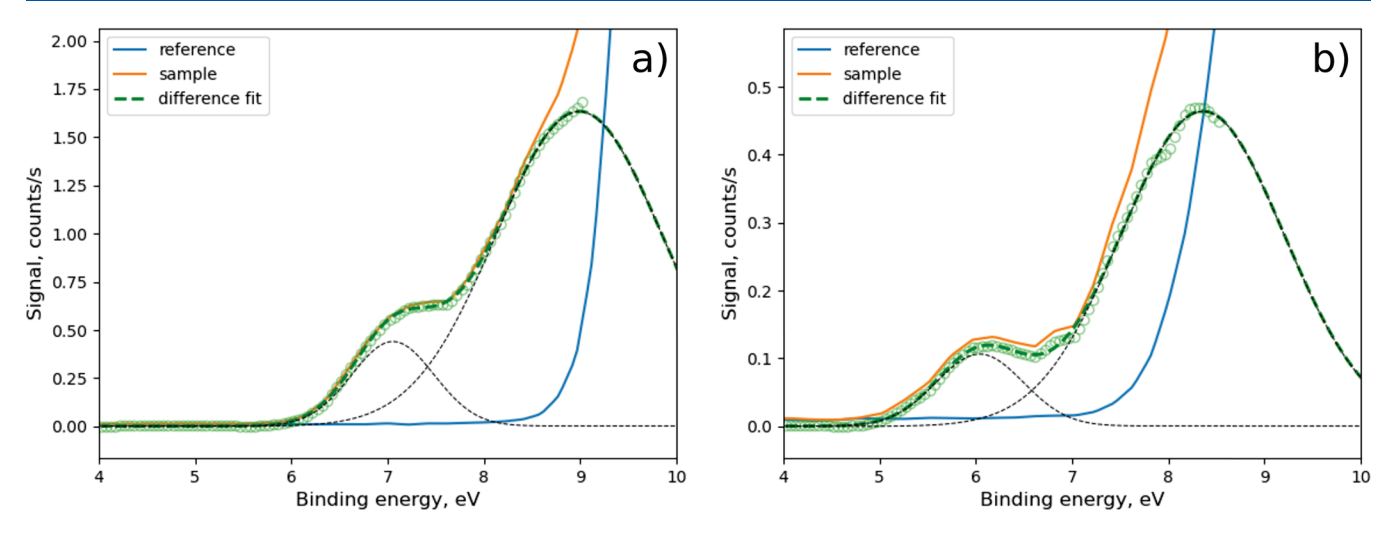


**Figure 4.** (a) Photoelectron spectrum of NAIP. The sample and solvent spectra are shown as orange and blue lines, respectively. The difference spectrum (green open circles) shows two bands and is well-described by two Gaussian profiles (green dashed curve). The individual Gaussians are shown with black dashed lines. The central binding energies of the two bands are 7.1 and 9.0 eV. (b) Photoelectron spectrum of *p*-HDIOP. The central binding energies of the two bands are 6.0 and 8.4 eV.

Table 1. Computed Binding Energies of NAIP and p-HDIOP

Method <sup>a</sup>	Energy <sup>b</sup>	Solvation <sup>c</sup>	E-NAIP (eV)	Z-NAIP (eV)	E-p-HDIOP (eV)	Z-p-HDIOP (eV)	$\Delta(E\text{-NAIP} - E\text{-}p\text{-HDIOP})$
M1	$E^{\nu}$	None	10.6	10.6	2.8	2.6	7.8
M2	$E^{\nu}$	None	10.4	10.5	2.2	2.0	8.2
M3	$E^{\nu}$	None	10.7	10.8	2.8	2.7	7.9
M1	$E^a_{ee}$	None	10.5	10.5	2.7	2.5	7.8
M2	$E^a_{ee}$	None	10.3	10.3	2.1	1.9	8.1
M3	$E^a_{ee}$	None	10.6	10.6	2.7	2.6	7.9
M1	$E^a_{00}$	None	10.5	10.5	2.7	2.5	7.8
M1	$E^{ u}$	e-PCM	6.0	6.0	4.5	4.5	1.5
M1	$E^{ u}$	ne-PCM	6.9	6.9	5.5	5.5	1.4
M2	$E^{ u}$	ne-PCM	7.6	7.6	5.8	5.8	1.8
M1	$E^a_{ee}$	e-PCM	5.9	5.9	4.4	4.4	1.5
M1	$E_{00}^{a}$	e-PCM	5.9	5.9	4.5	4.4	1.4
M1	$E^{\nu}$	ASEC	7.7	7.7	6.7	6.7	1.0
M2	$E^{\nu}$	ASEC	7.7	7.6	6.3	6.3	1.4
M3	$E^{\nu}$	ASEC	7.8	7.8	7.0	7.0	0.8
M3-no ion	$E^{\nu}$	ASEC	8.4	8.4	6.3	6.4	2.1
Experiment			7.1		6.0		1.1

 $^a$ M1 =  $\Delta$ SCF, PBE0/6-311+G\*; M2 = EOM-IP-CCSD// $\omega$ B97X-D/cc-pVDZ; M3 = CASPT2/ANO-L-VDZP//CASSCF/6-31G\*.  $^b$ E $^v$  = Vertical binding energy,  $E^a_{ee}$  = Adiabatic binding energy,  $E^a_{00}$  = 0–0 binding energy.  $^c$ e-PCM = equilibrium PCM; ne-PCM = nonequilibrium PCM; ASEC = average solvent electrostatic configuration.

(related to probing depth), energy of the ionizing radiation, solvent, and angle of detection of the electrons. 6,85–88 It can be argued that inelastic scattering may only allow higher energy electrons to escape the solvent and therefore give an apparent binding energy higher than the true one. However, given that the photoelectron spectra can be fitted accurately using Gaussian curves in Figure 4, this suggests that scattering is not significant enough to distort the spectra. In any case, it is expected that the effect of electron loss is on the same order of magnitude as the experimental uncertainty at the ionizing radiation energy employed (23.4 eV and 16-17 eV above the ionization/detachment threshold for the two switches). Another factor is the sensitivity of the binding energy to the degree of solvation of the molecular switches; the switches near the air-water interface may have different binding energies compared to the bulk. However, a recent computational study indicates that the binding energy of ions is relatively insensitive

to a bulk versus interfacial solvation. <sup>89</sup> Finally, the computational methods employed here also have limitations; while implicit solvation may miss specific details of the solvent—solute interactions, the ASEC-FEG approach used here treats the solvent with a fixed-charge force field and misses solvent polarization effects.

A 10 mM NaCl solution was prepared and used both for the NAIP sample preparation and for reference solvent measurements performed before and after the sample measurements, which is important for background suppression, as discussed below. The NAIP sample thus contained 1.35 mM concentration of NAIP molecules and 10 mM NaCl in pure water. The total volume of the sample solution was 15 mL, which was sufficient for 15 min of signal accumulation at the flow rate of 0.4 mL/min after accounting for the volume of the sample delivery system. All the flasks and sample supply capillaries were covered by aluminum foil to prevent

compound isomerization under the laboratory light. The reference solvent measurements were taken for the same amount of time. The measured photoelectron spectrum of NAIP is shown in Figure 4a as an orange line together with the reference solvent spectrum (blue curve), plotted as a function of the binding energy (eBE, determined using the photon energy minus kinetic energy of the detected electrons). The empty circles show the difference spectrum resulting from subtraction of the solvent signal. The green dashed line represents a fit line composed of two Gaussian profiles, which describe well the two bands observed in the range of 5-9 eV. The central binding energies of the two bands are 7.1 and 9.0 eV. The full widths at half-maximum (FWHM) are 1.0 and 2.0 eV, respectively. The errors of the fits are on the order of 1% of the values, but systematic uncertainties (e.g., from the bandwidth of the XUV light) may be larger. From experience, we conservatively estimate them to be on the order of 0.2-0.3

The anionic *p*-HDIOP solution requires a basic solution of the otherwise neutral chromophore. Therefore, 100 mM KOH was added to the water solvent, which also contained 10 mM NaCl. This solution was used both for sample preparation and for reference measurements. The *p*-HDIOP sample thus contained 1.15 mM *p*-HDIOP, 100 mM KOH, and 10 mM NaCl in pure water. Other parameters of the measurement correspond to those of NAIP, as described above. The photoelectron spectra of *p*-HDIOP are shown in Figure 4b. Two bands are again observed in the signal of the solute. The two-Gaussian fit yields the central band positions of 6.0 and 8.4 eV with a FWHM of 1.1 and 2.0 eV, respectively. The solvent spectrum in Figure 4b is different from that of Figure 4a due to the weak OH<sup>-</sup> band observed in the range of 7–8 eV binding energies. This signal is removed by solvent signal subtraction.

The remainder of this Letter will focus on the first electron binding energy. The results of the gas-phase, PCM, and ASEC *ab initio* calculations for the three electronic structure methods are summarized in Table 1 along with the experimental results.

In the gas-phase calculations, NAIP and *p*-HDIOP have binding energies that differ by ca. 8 eV. This is not surprising considering their opposite charges; *p*-HDIOP is negatively charged and has a low photodetachment energy in the gas phase. NAIP is positively charged, and its ionization to the 2+ charged state requires significantly more energy.

Upon solvation, the negatively charged *p*-HDIOP is stabilized more than the neutral final state, which increases its binding energy relative to that of the gas phase. Conversely, solvation of NAIP is likely to have a larger stabilizing effect on the final (2+) state compared to the initial (1+) state, reducing the binding energy. Solvation therefore is expected to have a large and opposite effect on the binding energies of the two molecular switches. Indeed, the experimental results and the calculations in Table 1 indicate that accounting for the solvent environment brings the binding energies of NAIP and *p*-HDIOP much closer together, from 8 eV in the gas phase to ca. 1 eV in the aqueous phase.

Before discussing the effect of solvation, we looked at the gas-phase calculations to determine a suitable protocol for computing binding energies. The three electronic structure methods give mostly consistent vertical and adiabatic binding energies in the gas phase. Methods M1 and M3 in particular agree with each other to within 0.1–0.2 eV in all cases. M2 underestimates the binding energy of *p*-HDIOP compared with the other two methods. This can be attributed to the

missing diffuse basis functions in the EOM-IP-CCSD/cc-pVDZ calculations. Diffuse basis functions are important for accurately determining the energy of the negatively charged initial state of *p*-HDIOP. Accounting for those diffuse functions should increase the binding energy of *p*-HDIOP.

Comparing E- and Z-Isomers of NAIP and p-HDIOP. Previous studies have established that the E-stereoisomer is more stable than Z- for both NAIP and p-HDIOP. We computed  $E^v$  and  $E^a_{ee}$  for all four systems (E-NAIP, Z-NAIP, E-p-HDIOP, and Z-p-HDIOP). The computations show that binding energies for E- and Z-isomers for each of NAIP and p-HDIOP are close (within 0.1 eV for NAIP, and within 0.2 eV for p-HDIOP). Therefore, the stereoisomers cannot be resolved experimentally by using photoelectron spectroscopy. The remainder of the discussion will focus on the E-NAIP and E-p-HDIOP stereoisomers.

Comparing Vertical ( $E^{v}$ ), Adiabatic ( $E^{a}_{ee}$ ), and 0–0 ( $E^{a}_{00}$ ) Binding Energies.  $E^{a}_{ee}$  was computed using methods M1, M2, and M3 in the gas phase. In all cases, the effect of geometry relaxation of the ionized state reduced the binding energy to under 0.2 eV compared to  $E^{v}$ . We accounted for the effect of ZPVE on adiabatic excitation energies for method M1. The ZPVEs are similar for the initial and ionized states (within 0.05 eV) and therefore give  $E^{a}_{00}$  energies that are similar to those for  $E^{a}_{ee}$ .

Of the three quantities  $(E^{\nu}, E^{a}_{ee})$  and  $E^{a}_{00}$ , only  $E^{a}_{00}$  has a direct connection to an experimental quantity. In a wellresolved spectrum for a vibrationally cold molecule,  $E_{00}^a$ corresponds to the lowest-energy transition and marks the onset of the spectral band. The other two quantities are theoretical, although  $E^{\nu}$  can be (and often is) connected to the energy where the absorption or emission signal is at a maximum for that band. Given the similarity of calculated  $E^{\nu}$ and  $E_{00}^a$  for each of p-HDIOP and NAIP, it appears that neither switch undergoes significant structural rearrangement upon ionization. This is in contrast to the behavior of these switches in the first singlet excited state, which quickly leads to a strong relaxation along bond-length alternation and out-of-plane deformation modes. <sup>27,28,91–93</sup> The remainder of the discussion will therefore focus on vertical binding energies  $(E^{\nu})$ , which will be compared to the experimentally determined central binding energies from the first bands in Figure 4.

Comparing Solvation Models. The  $E^{\nu}$  and  $\Delta E^{\nu}$  results from Table 1 are plotted in Figure 5. The binding energies of NAIP and p-HDIOP differ by about 8 eV in the gas phase. Using an equilibrium implicit PCM model decreases this  $\Delta E^{\nu}$  to 1.5 eV for M1, which is comparable to the experimental difference of binding energies ( $\Delta eBE$ ) value of 1.1 eV. Using a polarizable continuum model therefore largely captures the effect of solvation on those two oppositely charged molecules. However, equilibrium PCM calculations underestimate the absolute binding energies of both switches relative to the experimental ones by over 1 eV. This is not surprising; e-PCM fully relaxes the solvent environment in the ionized state, which is an incorrect representation of the solvent response to sudden ionization. The ionized state energy is therefore overstabilized, and the binding energy is underestimated.

This underestimation of the binding energy is largely resolved by using a nonequilibrium PCM approach. ne-PCM calculations using both M1 and M2 give binding energies that are in better agreement with those obtained experimentally (within 0.5 eV). The computed  $\Delta E^{\nu}$ 's for M1 using ne-PCM are also slightly improved, at 1.4 eV compared to the

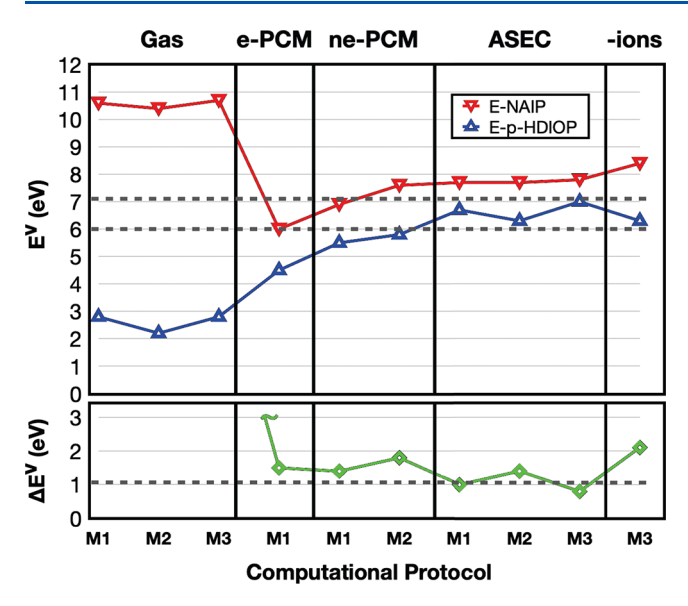


Figure 5. (Top) Computed  $E^{\nu}$ 's for E-NAIP (red) and E-p-HDIOP (blue) using the computational methods and solvation models, as shown in Table 1. (Bottom) A plot of the difference (green) in the  $E^{\nu}$  for E-NAIP and E-p-HDIOP ( $\Delta E^{\nu}$ ) as a function of the method and solvation model. The horizontal dashed lines indicate the experimental values.

experimental 1.1 eV. For M2, the  $\Delta E^{\nu}$  is overestimated, at 1.8 eV, but this could be explained again by the missing diffuse basis functions, which leads to an underestimation of the *p*-HDIOP binding energy.

ASEC-FEG QM/MM explicit solvent calculations further reduce the computed  $\Delta E^{\nu}$  to 0.8–1.4 eV, in good agreement with the experimental  $\Delta eBE$ . The result from M1 is in particularly good agreement, at 1.0 eV, while M2 overestimates  $\Delta E^{\nu}$  (due to the basis set), and M3 underestimates  $\Delta E^{\nu}$ . Nonetheless, all three models are within 0.3 eV of the experimental  $\Delta IE$ . On the other hand, while the ASEC-FEG QM/MM calculations give a  $\Delta E^{\nu}$  that is in good agreement with the experiment, all three methods (M1, M2, and M3) overestimate the absolute binding energies of both NAIP and p-HDIOP by over 0.5 eV. This is on the order of magnitude of the effect of solvent polarization, which can exceed 0.5 eV,  $^{26,94,95}$  and is missing in the ASEC fixed charge model used here.

Effect of the Counterion. Although both ne-PCM and ASEC-FEG give binding energies that are in reasonably good agreement with the experiment, it would be interesting to look at one of the aspects where the ASEC and PCM solvation models differ; ASEC includes not only explicit solvent but also explicit counterions. The ASEC configuration samples the distribution of those ions from the MD simulation. Figure 6 shows the radial distribution functions (RDF) and cumulative number (CN) of the counterion relative to the center of mass of the switches computed from one of the MD simulations.

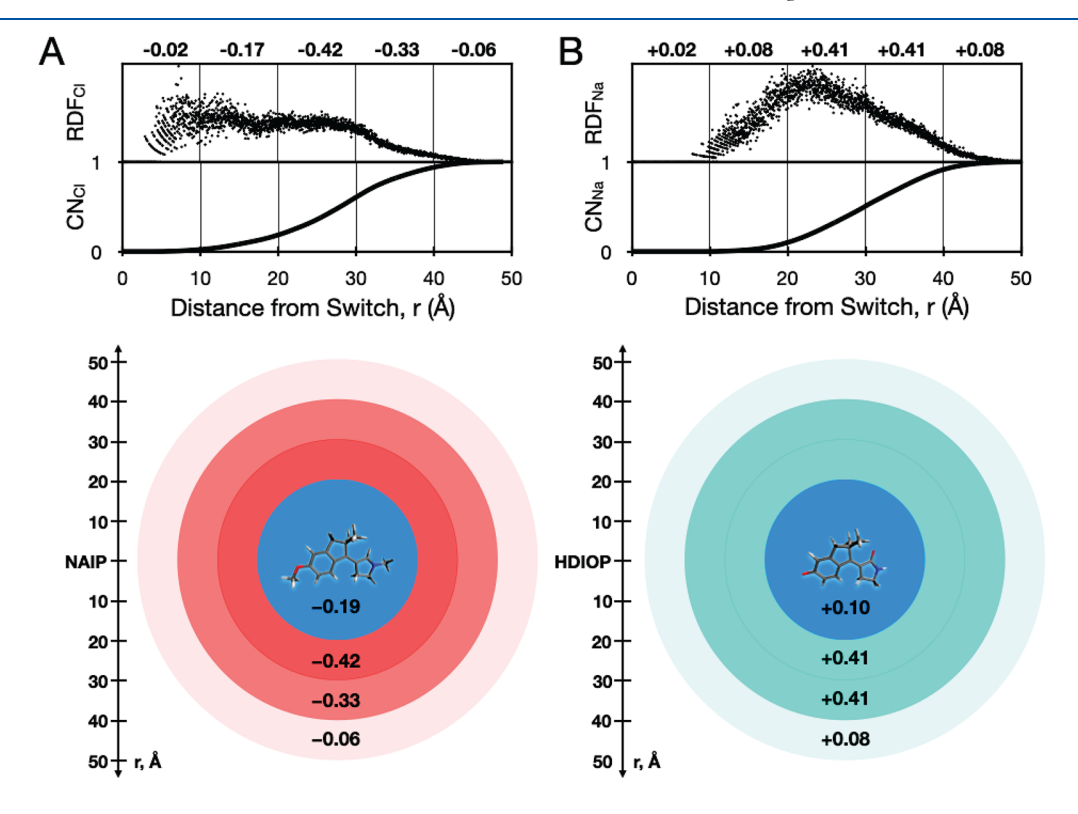


Figure 6. (Top) Radial distribution functions (RDF) and cumulative number (CN) of the counterion for E-NAIP (A) and Z-p-HDIOP (B). The RDF and CN for each of the two systems were computed from a 4 ns MD simulation. The CN converges to 1 at a large radius because there is only one counterion and therefore represents the probability of finding the counterion at a given value of r. The numbers at the top indicate the probability of finding the counterion in each 10 Å shell around the center of mass of the molecule multiplied by the sign of the charge. (Bottom) Schematic representation of an ASEC configuration that shows how the counterion is distributed. The blue circle represents the water solvent ASEC configuration, which is explicitly included in the QM/MM calculations for up to 20 Å. The surrounding concentric circles represent the counterions that interact at a long range with the solute. The color and shading of each shell relate to the total charge within that spherical shell, based on the CNs computed from an MD simulation.

From this distribution of charges, it is possible to estimate the effect of the ions using Coulomb's law. Assuming a centrosymmetric potential interacting with a point charge of magnitude e, and in the absence of a dielectric medium

$$V = -\frac{1}{4\pi\epsilon_0} \int \frac{\rho(r)}{r} d\tau \tag{1}$$

The  $\rho(r)$  term can be represented by using the CN plots in Figure 6. Integrating the expression above using these CN plots gives an energy of 0.52 eV for the interaction between Na<sup>+</sup> ions and the negatively charged p-HDIOP, and 0.60 eV for the interaction between Cl<sup>-</sup> ions and positively charged NAIP. Considering that this charge interaction will stabilize the 2+ ionized state more than the 1+ initial state in NAIP, but will instead stabilize the -1 initial state in p-HDIOP more than the neutral state, the direct effect of counterions on  $\Delta E^{\nu}$  is over 1 eV. Indeed, we find that simply deleting the counterions and repeating the QM/MM calculations increases the computed  $\Delta E^{\nu}$  from 0.8 to 2.1 eV (M3-no ion in Table 1).

Of course, deleting the counterions does not give a realistic representation of the effect they have on the binding energy. The calculations only account for a minimal number of counterions of the solute, while experimental solutions are more complex and contain NaCl and KOH for experimental purposes. Further, water molecules are arranged in such a way to screen the counterions and will rearrange in the absence of these counterion. If we account for the relative permittivity of water (78.4 at ambient conditions), then the effect of the counterions on the binding energy of the molecular switches would be substantially diminished. However, NAIP and p-HDIOP are not point charges in a uniform dielectric field, and the counterion distribution is certainly not centro-symmetric. Therefore, counterions in the ASEC-FEG model may contribute to long-range electrostatic solute-counterion interactions that are missing in the PCM models, leading to a slightly lower computed  $\Delta eBE$ . Such long-range effects were found to be important in QM/MM calculations of proteins such as rhodopsins and flavoprotein photoreceptors, 72,96 where counterions are distributed near the surface of the protein. More realistic models of the solute-ion interactions will be addressed in a future work.

In conclusion, we have presented experimental XPS and computed binding energies of a positively charged molecule, NAIP, and a negatively charged molecule, p-HDIOP. These photoswitches pose a challenge to electronic structure calculations, which need to account for large and opposite solvation effects through suitable solvation models. Experimentally, the difference in electron binding energy ( $\Delta eBE$ ) between p-HDIOP and NAIP is 1.1 eV, compared to the ca. 8 eV difference predicted in the gas phase. Nonequilibrium implicit (ne-PCM) solvation models capture a large part of the solvent effect and give both absolute and relative binding energies that are in good agreement with the experiments. Equilibrium (e-PCM) models reproduce the relative binding energies of the two switches relatively well ( $\Delta eBE = 1.5 \text{ eV}$ ) but give underestimated binding energies by over 1 eV. ASEC-FEG explicit solvent models give a  $\Delta E^{\nu}$  of 0.8-1.4 eV, depending on the method, in closer agreement to the experimental ΔeBE. An advantage of the ASEC-FEG explicit solvent model is that it captures long-range electrostatic interactions with a time-averaged solvent and counterion environment. However, it misses fast polarization effects of the nearby solvent molecules, which are better captured by ne-PCM solvent models. The results presented in this work will serve as a solid basis for time-resolved XPS experiments, which are being performed in our laboratory.

#### ASSOCIATED CONTENT

#### **Data Availability Statement**

The data that support the findings of this study are available from the corresponding author upon reasonable request.

# **Solution** Supporting Information

The Supporting Information is available free of charge at https://pubs.acs.org/doi/10.1021/acs.jpclett.3c00828.

Details of the QM/MM calculations, tables of computed absolute and vertical binding energies, and optimized coordinates for the ground and ionized states of the molecular switches (PDF)

# AUTHOR INFORMATION

### **Corresponding Authors**

- O. Kornilov Max Born Institute, 12489 Berlin, Germany; orcid.org/0000-0002-3343-2614; Email: kornilov@mbiberlin.de
- S. Gozem Georgia State University, Atlanta, Georgia 30303, United States; oorcid.org/0000-0002-6429-2853; Email: sgozem@gsu.edu

#### **Authors**

- E. Ikonnikov Max Born Institute, 12489 Berlin, Germany M. Paolino Department of Biotechnology, Chemistry and Pharmacy, University of Siena, I-53100 Siena, Italy; orcid.org/0000-0003-1387-7875
- J. C. Garcia-Alvarez Georgia State University, Atlanta, Georgia 30303, United States
- Y. Orozco-Gonzalez Georgia State University, Atlanta, Georgia 30303, United States; orcid.org/0000-0001-7225-2424
- C. Granados Max Born Institute, 12489 Berlin, Germany
- A. Röder Max Born Institute, 12489 Berlin, Germany
- J. Léonard Strasbourg Institute of Material Physics and Chemistry, University of Strasbourg - CNRS, 67000 Strasbourg, France
- M. Olivucci Department of Biotechnology, Chemistry and Pharmacy, University of Siena, I-53100 Siena, Italy; orcid.org/0000-0002-8247-209X
- S. Haacke Strasbourg Institute of Material Physics and Chemistry, University of Strasbourg - CNRS, 67000 Strasbourg, France

Complete contact information is available at: https://pubs.acs.org/10.1021/acs.jpclett.3c00828

#### **Notes**

The authors declare no competing financial interest.

#### ACKNOWLEDGMENTS

This material is based upon work supported by the National Science Foundation (NSF) under Grant CHE-2047667 (S.G.). We also acknowledge NSF XSEDE for computational resources from Research Allocation CHE180027 and the Advanced Research Computing Technology and Innovation Core (ARCTIC) resources at Georgia State University's Research Solutions, made available by the National Science Foundation Major Research Instrumentation (MRI) Grant

Number CNS-1920024. J.C.G.-A. acknowledges the Molecular Basis of Disease Program fellowship from Georgia State University. E.I., C.G., and O.K. acknowledge the support of the Deutsche Forschungsgemeinschaft (Grant KO 4920/1-1). A.R. acknowledges support of the Alexander von Humboldt Foundation. S.H. is grateful to the Strasbourg Foundation J.-M. Lehn, the CNRS program "Emerging Int. Actions" and to the German Academic Exchange Service (DAAD) for financial support.

# REFERENCES

- (1) Winter, B.; Faubel, M. Photoemission from liquid aqueous solutions. *Chemical reviews* **2006**, *106*, 1176–1211.
- (2) Seidel, R.; Thurmer, S.; Winter, B. Photoelectron spectroscopy meets aqueous solution: studies from a vacuum liquid microjet. *The Journal of Physical Chemistry Letters* **2011**, *2*, 633–641.
- (3) Salmeron, M.; Schlögl, R. Ambient pressure photoelectron spectroscopy: A new tool for surface science and nanotechnology. *Surface Science Reports* **2008**, *63*, 169–199.
- (4) Seidel, R.; Winter, B.; Bradforth, S. E. Valence electronic structure of aqueous solutions: Insights from photoelectron spectroscopy. *Annual review of physical chemistry* **2016**, *67*, 283–305.
- (5) Henley, A.; Fielding, H. H. Anion photoelectron spectroscopy of protein chromophores. *International Reviews in Physical Chemistry* **2019**, 38, 1–34.
- (6) Tau, O.; Henley, A.; Boichenko, A. N.; Kleshchina, N. N.; Riley, R.; Wang, B.; Winning, D.; Lewin, R.; Parkin, I. P.; Ward, J. M.; et al. Liquid-microjet photoelectron spectroscopy of the green fluorescent protein chromophore. *Nature communications* **2022**, *13*, 507.
- (7) Ojeda, J.; Arrell, C. A.; Longetti, L.; Chergui, M.; Helbing, J. Charge-transfer and impulsive electronic-to-vibrational energy conversion in ferricyanide: ultrafast photoelectron and transient infrared studies. *Phys. Chem. Chem. Phys.* **2017**, *19*, 17052–17062.
- (8) Engel, N.; Bokarev, S. I.; Moguilevski, A.; Raheem, A. A.; Al-Obaidi, R.; Möhle, T.; Grell, G.; Siefermann, K. R.; Abel, B.; Aziz, S. G.; et al. Light-induced relaxation dynamics of the ferricyanide ion revisited by ultrafast XUV photoelectron spectroscopy. *Phys. Chem. Chem. Phys.* **2017**, *19*, 14248–14255.
- (9) Hummert, J.; Reitsma, G.; Mayer, N.; Ikonnikov, E.; Eckstein, M.; Kornilov, O. Femtosecond Extreme Ultraviolet Photoelectron Spectroscopy of Organic Molecules in Aqueous Solution. *The Journal of Physical Chemistry Letters* **2018**, *9*, 6649–6655.
- (10) Longetti, L.; Randulová, M.; Ojeda, J.; Mewes, L.; Miseikis, L.; Grilj, J.; Sanchez-Gonzalez, A.; Witting, T.; Siegel, T.; Diveki, Z.; et al. Photoemission from non-polar aromatic molecules in the gas and liquid phase. *Phys. Chem. Chem. Phys.* **2020**, 22, 3965–3974.
- (11) Titov, E.; Hummert, J.; Ikonnikov, E.; Mitrić, R.; Kornilov, O. Electronic relaxation of aqueous aminoazobenzenes studied by time-resolved photoelectron spectroscopy and surface hopping TDDFT dynamics calculations. *Faraday Discuss.* **2021**, 228, 226–241.
- (12) Orimo, N.; Yamamoto, Y.-i.; Karashima, S.; Boyer, A.; Suzuki, T. Ultrafast Electronic Relaxation in 6-Methyluracil and 5-Fluorouracil in Isolated and Aqueous Conditions: Substituent and Solvent Effects. *The Journal of Physical Chemistry Letters* **2023**, 14, 2758–2763.
- (13) Pederson, J. P.; McDaniel, J. G. DFT-based QM/MM with particle-mesh Ewald for direct, long-range electrostatic embedding. *The Journal of Chemical Physics* **2022**, *156*, 174105.
- (14) Tazhigulov, R. N.; Bravaya, K. B. Free energies of redox half-reactions from first-principles calculations. *The Journal of Physical Chemistry Letters* **2016**, *7*, 2490–2495.
- (15) Warshel, A.; Dryga, A. Simulating electrostatic energies in proteins: Perspectives and some recent studies of pKas, redox, and other crucial functional properties. *Proteins: Structure, Function, and Bioinformatics* **2011**, 79, 3469–3484.
- (16) Jacobson, L. D.; Herbert, J. M. A one-electron model for the aqueous electron that includes many-body electron-water polarization: Bulk equilibrium structure, vertical electron binding energy,

- and optical absorption spectrum. The Journal of chemical physics 2010, 133, 154506.
- (17) Ghosh, D.; Roy, A.; Seidel, R.; Winter, B.; Bradforth, S.; Krylov, A. I. First-principle protocol for calculating ionization energies and redox potentials of solvated molecules and ions: theory and application to aqueous phenol and phenolate. *The Journal of Physical Chemistry B* **2012**, *116*, 7269–7280.
- (18) Ghosh, D.; Isayev, O.; Slipchenko, L. V.; Krylov, A. I. Effect of solvation on the vertical ionization energy of thymine: From microhydration to bulk. *The Journal of Physical Chemistry A* **2011**, 115, 6028–6038.
- (19) Herbert, J. M. Dielectric continuum methods for quantum chemistry. Wiley Interdisciplinary Reviews: Computational Molecular Science 2021, 11, e1519.
- (20) You, Z.-Q.; Mewes, J.-M.; Dreuw, A.; Herbert, J. M. Comparison of the Marcus and Pekar partitions in the context of non-equilibrium, polarizable-continuum solvation models. *The Journal of Chemical Physics* **2015**, *143*, 204104.
- (21) Cammi, R.; Tomasi, J. Nonequilibrium solvation theory for the polarizable continuum model: a new formulation at the SCF level with application to the case of the frequency-dependent linear electric response function. *Int. J. Quantum Chem.* **1995**, *56*, 465–474.
- (22) Aguilar, M.; Olivares del Valle, F.; Tomasi, J. Nonequilibrium solvation: An ab initio quantum-mechanical method in the continuum cavity model approximation. *The Journal of chemical physics* **1993**, *98*, 7375–7384.
- (23) Mennucci, B.; Cammi, R.; Tomasi, J. Excited states and solvatochromic shifts within a nonequilibrium solvation approach: A new formulation of the integral equation formalism method at the self-consistent field, configuration interaction, and multiconfiguration self-consistent field level. *The Journal of chemical physics* **1998**, *109*, 2798–2807.
- (24) Coons, M. P.; Herbert, J. M. Quantum chemistry in arbitrary dielectric environments: Theory and implementation of nonequilibrium Poisson boundary conditions and application to compute vertical ionization energies at the air/water interface. *The Journal of chemical physics* **2018**, *148*, 222834.
- (25) Coons, M. P.; You, Z.-Q.; Herbert, J. M. The hydrated electron at the surface of neat liquid water appears to be indistinguishable from the bulk species. *J. Am. Chem. Soc.* **2016**, *138*, 10879–10886.
- (26) Tazhigulov, R. N.; Gurunathan, P. K.; Kim, Y.; Slipchenko, L. V.; Bravaya, K. B. Polarizable embedding for simulating redox potentials of biomolecules. *Phys. Chem. Chem. Phys.* **2019**, *21*, 11642–11650.
- (27) Sinicropi, A.; Martin, E.; Ryazantsev, M.; Helbing, J.; Briand, J.; Sharma, D.; Léonard, J.; Haacke, S.; Cannizzo, A.; Chergui, M.; et al. An artificial molecular switch that mimics the visual pigment and completes its photocycle in picoseconds. *Proceedings of the National Academy of Sciences* **2008**, *105*, 17642–17647.
- (28) Gueye, M.; Manathunga, M.; Agathangelou, D.; Orozco, Y.; Paolino, M.; Fusi, S.; Haacke, S.; Olivucci, M.; Léonard, J. Engineering the vibrational coherence of vision into a synthetic molecular device. *Nature communications* **2018**, *9*, 313.
- (29) Paolino, M.; Gueye, M.; Pieri, E.; Manathunga, M.; Fusi, S.; Cappelli, A.; Latterini, L.; Pannacci, D.; Filatov, M.; Léonard, J.; et al. Design, synthesis, and dynamics of a green fluorescent protein fluorophore mimic with an ultrafast switching function. *J. Am. Chem. Soc.* 2016, 138, 9807–9825.
- (30) Dunkelberger, A. D.; Kieda, R. D.; Shin, J. Y.; Rossi Paccani, R.; Fusi, S.; Olivucci, M.; Fleming Crim, F. Photoisomerization and relaxation dynamics of a structurally modified biomimetic photoswitch. *The Journal of Physical Chemistry A* **2012**, *116*, 3527–3533.
- (31) Adamo, C.; Barone, V. Toward reliable density functional methods without adjustable parameters: The PBE0 model. *The Journal of chemical physics* **1999**, *110*, 6158–6170.
- (32) Ernzerhof, M.; Scuseria, G. E. Assessment of the Perdew-Burke-Ernzerhof exchange-correlation functional. *The Journal of chemical physics* **1999**, *110*, 5029–5036.

- (33) Epifanovsky, E.; Gilbert, A. T. B.; Feng, X.; Lee, J.; Mao, Y.; Mardirossian, N.; Pokhilko, P.; White, A. F.; Coons, M. P.; Dempwolff, A. L.; et al. Software for the frontiers of quantum chemistry: An overview of developments in the Q-Chem 5 package. *The Journal of Chemical Physics* **2021**, *155*, 084801.
- (34) Chai, J.-D.; Head-Gordon, M. Long-range corrected hybrid density functionals with damped atom-atom dispersion corrections. *Phys. Chem. Phys.* **2008**, *10*, 6615–6620.
- (35) Dunning, T. H., Jr Gaussian basis sets for use in correlated molecular calculations. I. The atoms boron through neon and hydrogen. *The Journal of chemical physics* **1989**, 90, 1007–1023.
- (36) Stanton, J. F.; Gauss, J. Analytic energy derivatives for ionized states described by the equation-of-motion coupled cluster method. *The Journal of chemical physics* **1994**, *101*, 8938–8944.
- (37) Krylov, A. I. Equation-of-motion coupled-cluster methods for open-shell and electronically excited species: The hitchhiker's guide to Fock space. *Annu. Rev. Phys. Chem.* **2008**, *59*, 433–462.
- (38) Pokhilko, P.; Epifanovsky, E.; Krylov, A. I. Double precision is not needed for many-body calculations: Emergent conventional wisdom. *Journal of chemical theory and computation* **2018**, *14*, 4088–4096.
- (39) Landau, A.; Khistyaev, K.; Dolgikh, S.; Krylov, A. I. Frozen natural orbitals for ionized states within equation-of-motion coupled-cluster formalism. *The Journal of chemical physics* **2010**, *132*, 014109.
- (40) Andersson, K.; Malmqvist, P. A.; Roos, B. O.; Sadlej, A. J.; Wolinski, K. Second-order perturbation theory with a CASSCF reference function. *J. Phys. Chem.* **1990**, *94*, 5483–5488.
- (41) Andersson, K.; Malmqvist, P.-Å.; Roos, B. O. Second-order perturbation theory with a complete active space self-consistent field reference function. *The Journal of chemical physics* **1992**, *96*, 1218–1226.
- (42) Melloni, A.; Rossi Paccani, R.; Donati, D.; Zanirato, V.; Sinicropi, A.; Parisi, M. L.; Martin, E.; Ryazantsev, M.; Ding, W. J.; Frutos, L. M.; et al. Modeling, preparation, and characterization of a dipole moment switch driven by Z/E photoisomerization. *J. Am. Chem. Soc.* **2010**, *132*, 9310–9319.
- (43) Gozem, S.; Huntress, M.; Schapiro, I.; Lindh, R.; Granovsky, A. A.; Angeli, C.; Olivucci, M. Dynamic electron correlation effects on the ground state potential energy surface of a retinal chromophore model. *Journal of chemical theory and computation* **2012**, *8*, 4069–4080
- (44) Gozem, S.; Melaccio, F.; Luk, H.; Rinaldi, S.; Olivucci, M. Learning from photobiology how to design molecular devices using a computer. *Chemical Society Reviews* **2014**, 43, 4019–4036.
- (45) Gozem, S.; Luk, H. L.; Schapiro, I.; Olivucci, M. Theory and simulation of the ultrafast double-bond isomerization of biological chromophores. *Chemical reviews* **2017**, *117*, 13502–13565.
- (46) Gallandi, L.; Marom, N.; Rinke, P.; Körzdörfer, T. Accurate ionization potentials and electron affinities of acceptor molecules II: non-empirically tuned long-range corrected hybrid functionals. *Journal of chemical theory and computation* **2016**, *12*, 605–614.
- (47) Kanchanakungwankul, S.; Truhlar, D. G. Examination of how well long-range-corrected density functionals satisfy the ionization energy theorem. *Journal of Chemical Theory and Computation* **2021**, 17, 4823–4830.
- (48) Pieniazek, P. A.; Arnstein, S. A.; Bradforth, S. E.; Krylov, A. I.; Sherrill, C. D. Benchmark full configuration interaction and equation-of-motion coupled-cluster model with single and double substitutions for ionized systems results for prototypical charge transfer systems: Noncovalent ionized dimers. *The Journal of chemical physics* **2007**, 127, 164110.
- (49) Bravaya, K. B.; Krylov, A. I. On the photodetachment from the green fluorescent protein chromophore. *The Journal of Physical Chemistry A* **2013**, *117*, 11815–11822.
- (50) Bravaya, K. B.; Epifanovsky, E.; Krylov, A. I. Four bases score a run: Ab initio calculations quantify a cooperative effect of H-bonding and π-stacking on the ionization energy of adenine in the AATT tetramer. *The Journal of Physical Chemistry Letters* **2012**, *3*, 2726–2732.

- (51) Woodhouse, J. L.; Henley, A.; Lewin, R.; Ward, J. M.; Hailes, H. C.; Bochenkova, A. V.; Fielding, H. H. A photoelectron imaging study of the deprotonated GFP chromophore anion and RNA fluorescent tags. *Phys. Chem. Chem. Phys.* **2021**, 23, 19911–19922.
- (52) Hendrickx, M.; Clima, S. Adiabatic electron affinities of ScC2 and ScC3 evaluated by a multiconfigurational approach. *Chem. Phys. Lett.* **2004**, 388, 284–289.
- (53) Clima, S.; Hendrickx, M. F. Interpretation of the photoelectron spectra of FeS2-by a multiconfiguration computational approach. *The Journal of Physical Chemistry A* **2007**, *111*, 10988–10992.
- (54) Boichenko, A. N.; Bochenkova, A. V. Accurate Vertical Electron Detachment Energies and Multiphoton Resonant Photoelectron Spectra of Biochromophore Anions in Aqueous Solution. *Journal of Chemical Theory and Computation* **2023**, DOI: 10.1021/acs.jctc.2c01082
- (55) Anstöter, C. S.; Gartmann, T. E.; Stanley, L. H.; Bochenkova, A. V.; Verlet, J. R. Electronic structure of the para-dinitrobenzene radical anion: a combined 2D photoelectron imaging and computational study. *Phys. Chem. Chem. Phys.* **2018**, *20*, 24019–24026.
- (56) Widmark, P.-O.; Malmqvist, P.-Å.; Roos, B. O. Density matrix averaged atomic natural orbital (ANO) basis sets for correlated molecular wave functions: I. First row atoms. *Theoretica chimica acta* 1990, 77, 291–306.
- (57) Aquilante, F.; Malmqvist, P.-Å.; Pedersen, T. B.; Ghosh, A.; Roos, B. O. Cholesky decomposition-based multiconfiguration second-order perturbation theory (CD-CASPT2): application to the spin-state energetics of CoIII (diiminato)(NPh). *Journal of chemical theory and computation* **2008**, *4*, 694–702.
- (58) Aquilante, F.; Autschbach, J.; Baiardi, A.; Battaglia, S.; Borin, V. A.; Chibotaru, L. F.; Conti, I.; De Vico, L.; Delcey, M.; Fdez. Galván, I.; et al. Modern quantum chemistry with [Open] Molcas. *The Journal of chemical physics* **2020**, *152*, 214117.
- (59) Schaftenaar, G.; Noordik, J. H. Molden: a pre-and post-processing program for molecular and electronic structures. *Journal of computer-aided molecular design* **2000**, *14*, 123–134.
- (60) Barone, V.; Cossi, M. Quantum calculation of molecular energies and energy gradients in solution by a conductor solvent model. *The Journal of Physical Chemistry A* **1998**, *102*, 1995–2001.
- (61) Cossi, M.; Rega, N.; Scalmani, G.; Barone, V. Energies, structures, and electronic properties of molecules in solution with the C-PCM solvation model. *Journal of computational chemistry* **2003**, 24, 669–681
- (62) Brady, J. E.; Carr, P. W. An analysis of dielectric models of solvatochromism. *The Journal of Physical Chemistry* **1985**, 89, 5759–5766.
- (63) Cossi, M.; Barone, V. Separation between fast and slow polarizations in continuum solvation models. *The Journal of Physical Chemistry A* **2000**, *104*, 10614–10622.
- (64) Mewes, J.-M.; You, Z.-Q.; Wormit, M.; Kriesche, T.; Herbert, J. M.; Dreuw, A. Experimental benchmark data and systematic evaluation of two a posteriori, polarizable-continuum corrections for vertical excitation energies in solution. *The Journal of Physical Chemistry A* **2015**, *119*, 5446–5464.
- (65) Coutinho, K.; Georg, H.; Fonseca, T.; Ludwig, V.; Canuto, S. An efficient statistically converged average configuration for solvent effects. *Chemical physics letters* **2007**, 437, 148–152.
- (66) Georg, H. C.; Canuto, S. Electronic properties of water in liquid environment. A sequential QM/MM study using the free energy gradient method. *The Journal of Physical Chemistry B* **2012**, *116*, 11247–11254.
- (67) Bistafa, C.; Georg, H. C.; Canuto, S. Combining ab initio multiconfigurational and Free Energy Gradient methods to study the  $\pi$ - $\pi$ \*excited state structure and properties of uracil in water. Computational and Theoretical Chemistry **2014**, 1040, 312–320.
- (68) Franco, L. R.; Brandão, I.; Fonseca, T. L.; Georg, H. C. Elucidating the structure of merocyanine dyes with the ASEC-FEG method. Phenol blue in solution. *The Journal of chemical physics* **2016**, 145, 194301.

- (69) Orozco-Gonzalez, Y.; Manathunga, M.; Marín, M. D. C.; Agathangelou, D.; Jung, K.-H.; Melaccio, F.; Ferré, N.; Haacke, S.; Coutinho, K.; Canuto, S.; et al. An average solvent electrostatic configuration protocol for Qm/mm free energy optimization: Implementation and application to rhodopsin systems. *Journal of chemical theory and computation* 2017, 13, 6391–6404.
- (70) Nikolaev, D. M.; Manathunga, M.; Orozco-Gonzalez, Y.; Shtyrov, A. A.; Guerrero Martinez, Y. O.; Gozem, S.; Ryazantsev, M. N.; Coutinho, K.; Canuto, S.; Olivucci, M. Free Energy Computation for an Isomerizing Chromophore in a Molecular Cavity via the Average Solvent Electrostatic Configuration Model: Applications in Rhodopsin and Rhodopsin-Mimicking Systems. *Journal of Chemical Theory and Computation* **2021**, *17*, 5885–5895.
- (71) Iyer, A.; Reis, R. A.; Gannavaram, S.; Momin, M.; Spring-Connell, A. M.; Orozco-Gonzalez, Y.; Agniswamy, J.; Hamelberg, D.; Weber, I. T.; Gozem, S.; et al. A Single-Point Mutation in d-Arginine Dehydrogenase Unlocks a Transient Conformational State Resulting in Altered Cofactor Reactivity. *Biochemistry* **2021**, *60*, 711–724.
- (72) Dratch, B. D.; Orozco-Gonzalez, Y.; Gadda, G.; Gozem, S. Ionic Atmosphere Effect on the Absorption Spectrum of a Flavoprotein: A Reminder to Consider Solution Ions. *The Journal of Physical Chemistry Letters* **2021**, *12*, 8384–8396.
- (73) Kabir, M. P.; Ouedraogo, D.; Orozco-Gonzalez, Y.; Gadda, G.; Gozem, S. Alternative Strategy for Spectral Tuning of Flavin-Binding Fluorescent Proteins. *The Journal of Physical Chemistry B* **2023**, 127, 1301–1311.
- (74) Galván, I. F.; Sánchez, M.; Martín, M.; Olivares del Valle, F.; Aguilar, M. Geometry optimization of molecules in solution: joint use of the mean field approximation and the free-energy gradient method. *The Journal of chemical physics* **2003**, *118*, 255–263.
- (75) König, G.; Mei, Y.; Pickard, F. C., IV; Simmonett, A. C.; Miller, B. T.; Herbert, J. M.; Woodcock, H. L.; Brooks, B. R.; Shao, Y. Computation of hydration free energies using the multiple environment single system quantum mechanical/molecular mechanical method. *Journal of chemical theory and computation* **2016**, *12*, 332–344.
- (76) Pickard, F. C., IV; König, G.; Simmonett, A. C.; Shao, Y.; Brooks, B. R. An efficient protocol for obtaining accurate hydration free energies using quantum chemistry and reweighting from molecular dynamics simulations. *Bioorganic & medicinal chemistry* **2016**, 24, 4988–4997.
- (77) Hess, B.; Kutzner, C.; Van Der Spoel, D.; Lindahl, E. GROMACS 4: algorithms for highly efficient, load-balanced, and scalable molecular simulation. *Journal of chemical theory and computation* **2008**, *4*, 435–447.
- (78) Bauer, P.; Hess, B.; Lindahl, E. GROMACS 2022.3 Manual; 2022.
- (79) Aquilante, F.; De Vico, L.; Ferré, N.; Ghigo, G.; Malmqvist, P.å.; Neogrády, P.; Pedersen, T. B.; Pitoňák, M.; Reiher, M.; Roos, B. O.; et al. MOLCAS 7: the next generation. *Journal of computational chemistry* **2010**, 31, 224–247.
- (80) Ponder, J. W.; Case, D. A. Force fields for protein simulations. *Advances in protein chemistry* **2003**, *66*, 27–85.
- (81) Ferré, N.; Olivucci, M. Probing the rhodopsin cavity with reduced retinal models at the CASPT2//CASSCF/AMBER level of theory. J. Am. Chem. Soc. 2003, 125, 6868–6869.
- (82) Rossi Paccani, R.; Donati, D.; Fusi, S.; Latterini, L.; Farina, G.; Zanirato, V.; Olivucci, M. Toward a stable  $\alpha$ -cycloalkyl amino acid with a photoswitchable cationic side chain. *The Journal of Organic Chemistry* **2012**, *77*, 1738–1748.
- (83) Eckstein, M.; Yang, C.-H.; Kubin, M.; Frassetto, F.; Poletto, L.; Ritze, H.-H.; Vrakking, M. J. J.; Kornilov, O. Dynamics of  $N_2$  Dissociation upon Inner-Valence Ionization by Wavelength-Selected XUV Pulses. *J. Phys. Chem. Lett.* **2015**, *6*, 419–425.
- (84) Thürmer, S.; Malerz, S.; Trinter, F.; Hergenhahn, U.; Lee, C.; Neumark, D. M.; Meijer, G.; Winter, B.; Wilkinson, I. Accurate vertical ionization energy and work function determinations of liquid water and aqueous solutions. *Chem. Sci.* **2021**, *12*, 10558–10582.

- (85) Michaud, M.; Wen, A.; Sanche, L. Cross sections for low-energy (1–100 eV) electron elastic and inelastic scattering in amorphous ice. *Radiation research* **2003**, *159*, 3–22.
- (86) Luckhaus, D.; Yamamoto, Y.-i.; Suzuki, T.; Signorell, R. Genuine binding energy of the hydrated electron. *Science advances* **2017**, 3, e1603224.
- (87) Dupuy, R.; Thürmer, S.; Richter, C.; Buttersack, T.; Trinter, F.; Winter, B.; Bluhm, H. Core-Level Photoelectron Angular Distributions at the Liquid-Vapor Interface. *Acc. Chem. Res.* **2023**, *56*, 215–223
- (88) Gozem, S.; Seidel, R.; Hergenhahn, U.; Lugovoy, E.; Abel, B.; Winter, B.; Krylov, A. I.; Bradforth, S. E. Probing the electronic structure of bulk water at the molecular length scale with angle-resolved photoelectron spectroscopy. *The Journal of Physical Chemistry Letters* **2020**, *11*, 5162–5170.
- (89) Paul, S. K.; Herbert, J. M. Probing Interfacial Effects on Ionization Energies: The Surprising Banality of Anion-Water Hydrogen Bonding at the Air/Water Interface. *J. Am. Chem. Soc.* **2021**, *143*, 10189–10202.
- (90) Gozem, S.; Krylov, A. I. The ezSpectra suite: An easy-to-use toolkit for spectroscopy modeling. Wiley Interdisciplinary Reviews: Computational Molecular Science 2022, 12, e1546.
- (91) Schapiro, I.; Fusi, S.; Olivucci, M.; Andruniów, T.; Sasidharanpillai, S.; Loppnow, G. R. Initial excited-state dynamics of an N-alkylated indanylidene-pyrroline (NAIP) rhodopsin analog. *The Journal of Physical Chemistry B* **2014**, *118*, 12243–12250.
- (92) Pooler, D. R.; Pierron, R.; Crespi, S.; Costil, R.; Pfeifer, L.; Léonard, J.; Olivucci, M.; Feringa, B. L. Effect of charge-transfer enhancement on the efficiency and rotary mechanism of an oxindole-based molecular motor. *Chemical Science* **2021**, *12*, 7486–7497.
- (93) Léonard, J.; Schapiro, I.; Briand, J.; Fusi, S.; Paccani, R. R.; Olivucci, M.; Haacke, S. Mechanistic origin of the vibrational coherence accompanying the photoreaction of biomimetic molecular switches. *Chem. Eur. J.* **2012**, *18*, 15296–15304.
- (94) Barrozo, A.; Xu, B.; Gunina, A. O.; Jacobs, M. I.; Wilson, K.; Kostko, O.; Ahmed, M.; Krylov, A. I. To be or not to be a molecular ion: the role of the solvent in photoionization of arginine. *The journal of physical chemistry letters* **2019**, *10*, 1860–1865.
- (95) Sadybekov, A.; Krylov, A. I. Coupled-cluster based approach for core-level states in condensed phase: Theory and application to different protonated forms of aqueous glycine. *The Journal of chemical physics* **2017**, *147*, 014107.
- (96) Pedraza-González, L.; De Vico, L.; Marín, M. d. C.; Fanelli, F.; Olivucci, M. a-ARM: automatic rhodopsin modeling with chromophore cavity generation, ionization state selection, and external counterion placement. *Journal of chemical theory and computation* **2019**, *15*, 3134–3152.